Ca^{2+}-Dependent Intracellular Drug Delivery System Developed with "Raspberry-Type" Particles-on-a-Particle Comprising Mesoporous Silica Core and α-Synuclein-Coated Gold Nanoparticles

Daekyun Lee,[†] Je Won Hong,[†] Chanyoung Park,[†] Hagyeol Lee,[†] Ji Eun Lee,[†,‡] Taeghwan Hyeon,[†,‡] and Seung R. Paik[†,*]

[†]School of Chemical and Biological Engineering, Institute of Chemical Processes, College of Engineering, Seoul National University, Seoul 151-744, Republic of Korea and [‡]Center for Nanoparticle Research, Institute for Basic Science, Seoul 151-744, Republic of Korea

ABSTRACT For the development of an intracellular cargo release system with mesoporous silica nanoparticles (MSN), gold nanoparticles coated with an amyloidogenic protein of α-synuclein were employed to prepare a protein-mediated nanocomposite into the "raspberry-type" particles-on-a-particle (PoP). The PoPs were successfully fabricated only at pH 4.4 by yielding the MSN coverage to 75.3% with 5 nm gold nanoparticles covalently coated with a mutant form of α-synuclein containing a cysteine residue at the C-terminus. The entrapped cargo of rhodamine 6G was shown to be selectively released from PoPs upon exposure to divalent cations including the α-synuclein-specific pathophysiological ligand of Ca^{2+}. Intracellular uptake of the PoPs preloaded with doxorubicin as an anticancer drug and its subsequent Ca^{2+}-dependent release were demonstrated with HeLa cells in the presence of intracellular Ca^{2+}-regulating agents. Therefore, the fabrication of PoPs with the self-interactive protein of α-synuclein is expected to serve as a platform technology for preparation of diversified nanocomposites with various nanoparticles and/or bioactive molecules for eventual applications in the areas of theranostics.

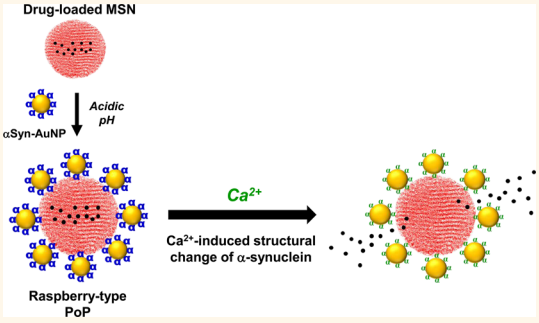

KEYWORDS: α-synuclein · controlled release · drug delivery · mesoporous silica nanoparticle · particles-on-a-particle

Efficient encapsulation, targeted delivery, and controlled release of drugs are prerequisite for designing advanced drug delivery system. In particular, the development of release-controllable delivery systems is important not only to avoid a substantial risk of systemic side effects due to constitutive release but also to greatly enhance the pharmacological effect of drugs at the target site.[1,2] Because of its unique porous architecture and versatility of surface chemistry along with biocompatibility, mesoporous silica nanoparticle (MSN) has been an attractive nanomaterial to be employed in drug delivery applications by retaining a large amount of cargo.[3−9] By shielding the pores of MSN with a variety of stimuli-responsive chemical entities as capping agents, the MSN-based delivery systems have been developed to regulate the retention and release of drugs.[10] For example, the assembly of polymers such as polyethylenimine[11] and poly(acrylic acid)[12] has been employed as a series of pH-responsive release systems. Such polymers tethered on the surface were producing supramolecular nanovalves that were easily disrupted in an acidic environment. A chemically labile disulfide linkage was also utilized to introduce the redox-responsive controlled release system into MSN.[13,14] Other external stimuli such as light and magnetic field have also been widely investigated to control the pore opening of mesoporous materials.[15,16] As the gatekeeping materials, small nanoparticles including CdS, Fe_3O_4, and Au have been employed to control the retention and release of cargo inside MSN.[17−21]

* Address correspondence to srpaik@snu.ac.kr.

Received for review December 22, 2013 and accepted August 28, 2014.

Published online August 28, 2014
10.1021/nn5034955

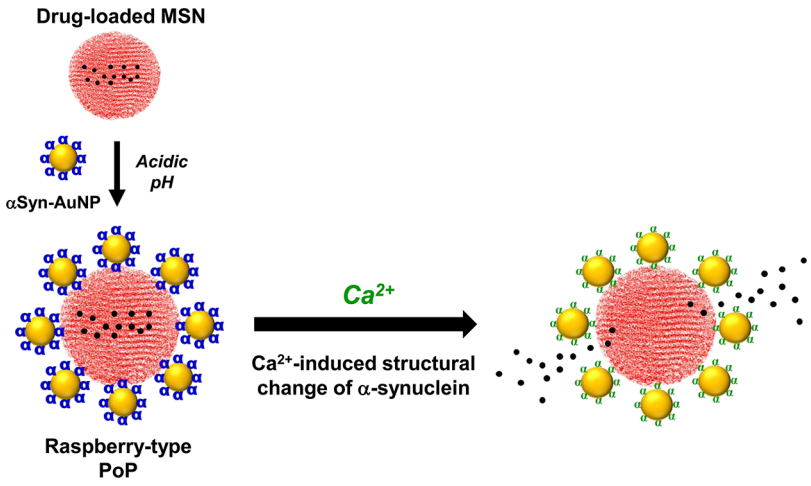

Figure 1. Schematic representation of "raspberry-type" PoPs and Ca^{2+}-triggered controlled release of cargo molecules.

In order to prepare a more efficient MSN-based drug-delivery system, however, the surface coverage of MSN by nanoparticles must be improved in addition to the fact that its gating should be controlled by pathophysiological agents other than acidic pH since cancerous tissues, for example, exhibit the acidic environment outside the cells, which would cause premature release of cancer drugs from their pH-sensitive carriers. By employing gold nanoparticles (AuNPs) coated with α-synuclein, an amyloidogenic protein responsible for the Lewy body formation in Parkinson's disease,[22] MSN has been covered with the protein-immobilized nanoparticles in high density. The resulting raspberry-type PoP nanocomposites have been shown to successfully entrap cargo molecules without premature leakage, and their release has been controlled by calcium ion as a pathophysiological ligand of α-synuclein (Figure 1). It has also been demonstrated that the PoPs could successfully deliver a chemotherapeutic agent of doxorubicin into cells and, thus, exhibit the cytotoxic effect through controlled release of the drug entrapped with cytosolic Ca^{2+}. Previously, we demonstrated that α-synuclein-coated AuNPs (αSyn-AuNPs) were assembled into a tightly packed monolayer on the surface of hydrophilic and hydroxyl-activated glass under acidic conditions, which would be attributed to the pH-induced structural change and self-interactive property of α-synuclein.[23] Therefore, the hydrophilic and silanol-rich MSN has been considered to provide the surface for the monolayer assembly of αSyn-AuNPs, which would produce the nanoparticle-capped MSN *via* a facile two-step procedure. Moreover, the α-synuclein introduced into PoP could play multiple roles offering a biocompatible surface to MSN, a ligand-sensitive switch to open the gates of MSN by altering its conformation, and additional modification sites to generate multifunctional MSN in addition to the simple anchoring of AuNPs to MSN.

RESULTS AND DISCUSSION

For the construction of PoP, the MSNs were synthesized to an average particle diameter of ~100 nm with channel-like mesoporous structures inside (pore diameter of 2−3 nm) as described in the previous report.[24] The cysteine mutant of recombinant human α-synuclein (Y136C) was immobilized on 10 nm AuNP surface to yield αSyn-AuNP. MSNs were then mixed with an excess amount of αSyn-AuNP (≥0.037 pmol of αSyn-AuNP per μg of MSN) in 10 mM citrate buffer (pH 4.4). In fact, the red particulates started to appear in solution within 5 min, and they eventually precipitated in 60 min, indicating the immediate assembly of αSyn-AuNPs on MSN (Figure 2a). As shown in the previous study,[23] this α-synuclein-mediated assembly of AuNPs on MSN occurred only at acidic pH, whereas most of the AuNPs remained in the supernatant at neutral or basic pH even after centrifugation (Figure 2b). However, bare AuNPs were not able to bind to MSN even at the acidic pH. The transmission electron microscope (TEM) clearly revealed the 10 nm αSyn-AuNPs uniformly distributed in monolayer on the surface of MSNs in the absence of any sort of nonspecific AuNP aggregates which were frequently found in other studies preparing nanoparticle-immobilized MSNs.[17−19] In terms of their appearance, therefore, our PoPs are unique by producing a "raspberry-type" nanostructure of AuNPs with the core of MSN. However, with the AuNPs immobilized with other mutant types of α-synuclein, S9C and A53C, those "raspberry-type" nanocomposites were not produced, thus indicating the importance of the exposed region of α-synuclein from AuNP for the PoP assembly (Figure S1, Supporting Information). We have measured zeta potentials of bare MSN and the AuNPs coated with α-synuclein in different orientations by employing three cysteine mutants of Y136C, A53C, and S9C. As pH changed from 6.5 to 4.4, the zeta potential of MSN increased drastically by almost 60% from −25.4 to −10.4 mV. While the AuNPs coated with

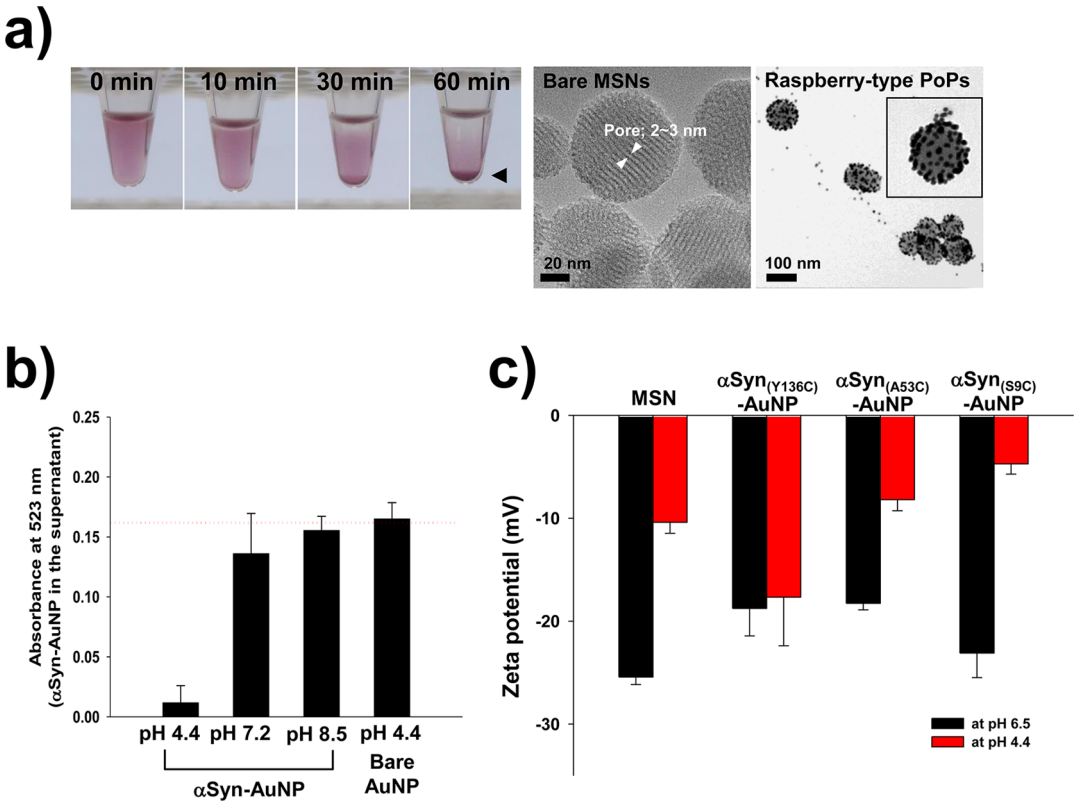

Figure 2. (a) Optical images of time-dependent "raspberry-type" PoP formation (top) and TEM images of bare MSN and PoP nanostructures (bottom). Mixture of MSNs and an excess amount of 10 nm αSyn-AuNPs (≥0.037 pmole of αSyn-AuNP/μg MSN) was incubated in 10 mM citrate (pH 4.4) for 30 min at room temperature. (b) pH-dependent assembly of αSyn-AuNP on MSN. Mixture of MSNs and αSyn-AuNPs was incubated at the buffer of indicated pH. The amount of free αSyn-AuNPs in the supernatant was measured with absorbance at 523 nm. The red dot line indicates the amount of αSyn-AuNP to be used for the PoP production. (c) Surface charge of MSN and αSyn-coated AuNPs. Zeta potentials of nanoparticles were measured in either 20 mM Mes or 10 mM citrate at pH 6.5 and 4.4, respectively.

either A53C or S9C also showed considerable change in zeta potentials as pH changed, the potential of the AuNPs coated with Y136C, which were the most effective αSyn-AuNP capable of producing PoPs, remained almost unchanged from −18.8 mV to −17.7 mV at pH 6.5 and 4.4, respectively (Figure 2c). Since PoPs have been successfully prepared only at pH 4.4 with the AuNPs conjugated with Y136C, the large decrease in the negative surface charge of MSN and no change in the charge of αSyn-AuNP appear to be critical for the PoP production. However, unlike other surface-coating simple polymers, the zeta potential of polypeptide with many ionizing groups and local noncovalent interactions does not allow us a straightforward interpretation. Nevertheless, a special molecular environment of mutant α-synuclein of Y136C on the surface of AuNP, whose net surface charge is resistant to the pH change, becomes suitable for the attachment to the acidified MSN by possibly eliciting selective local charge interactions.

The surface coverage of MSN by the AuNPs was expected to be improved as the AuNP sizes were varied for the PoP preparation. In fact, the numbers of AuNPs per MSN based on TEM images increased to 58 ± 11.1, 157 ± 8.1, and 300 ± 21.9 as the αSyn-AuNP sizes decreased to 20, 10, and 5 nm, respectively (Figure 3a). The packing density also increased to 0.52×10^3, 1.40×10^3, and 2.67×10^3 particles/μm^2, respectively, which might reflect the cargo retention capability of PoPs. The packing densities were determined by dividing the numbers of αSyn-AuNPs attached on MSN with its surface area which was calculated with the average hydrodynamic diameter of bare MSN as 189.1 ± 9.1 nm estimated with dynamic light scattering (DLS) analysis. Because of the highest surface coverage of MSN, most of the experiments in this study were performed using PoPs prepared with 5 nm αSyn-AuNPs unless indicated otherwise. The DLS data also showed that the resulting PoPs were not aggregated but well dispersed with an overall hydrodynamic diameter of 268.1 ± 34.9 nm (Figure S2, Supporting Information). These PoPs were also shown to be stable since they have maintained their structural integrity at physiological pH, temperature, and a high salt concentration of 1 M NaCl (Figure S3, Supporting Information). The Brunauer−Emmett−Teller (BET) analysis was also performed to find out how efficiently AuNPs were able to block the pores of MSN within the PoPs. The BET analysis of bare MSN showed a typical curve of N_2 adsorption/desorption isotherm giving rise to a surface area of 721 m^2/g and pore volume

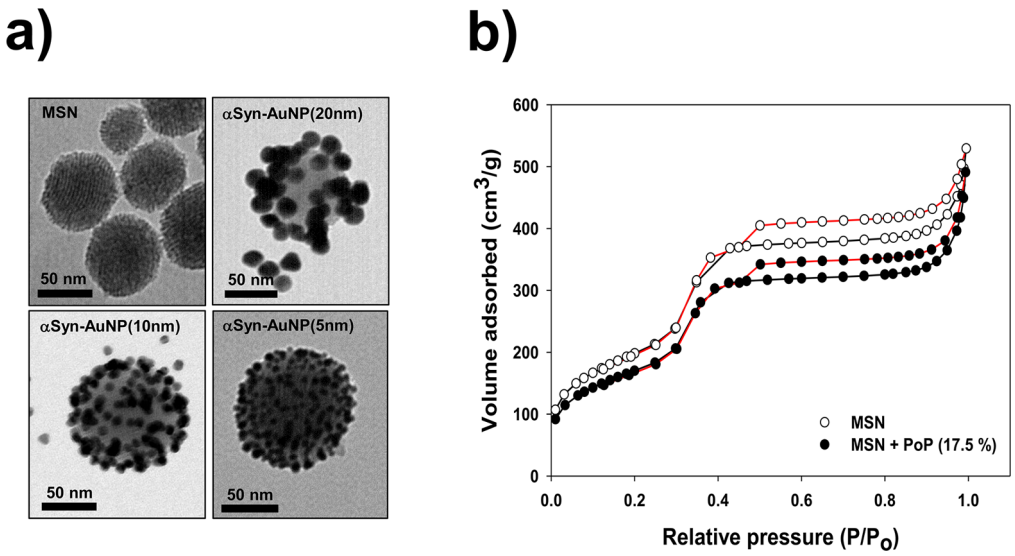

Figure 3. (a) TEM images of PoPs assembled with the αSyn-coated AuNPs of different sizes. (b) N_2 adsorption/desorption isotherms of PoPs. PoPs were constructed with 5 nm αSyn-AuNPs. The sample for BET analysis was prepared by mixing bare MSN with 17.5% of PoPs. Adsorption and desorption branches were represented by blank and red lines, respectively.

of 0.70 cm^3/g (Figure 3b). For the mixture of MSN and PoP (17.5%, w/w), however, the surface area and pore volume decreased to 621 m^2/g and 0.61 cm^3/g, respectively (Figure 3b). By considering a condition only with PoPs in the absence of bare MSN and the weight ratio of AuNP:MSN in PoPs (AuNP:MSN = 0.193:1), the surface area and pore volume of PoPs were estimated to be 179 m^2/g and 0.22 cm^3/g, respectively. Therefore, these data indicate that αSyn-AuNPs efficiently shield the pores of MSN in the PoP nanocomposites as the surface area and pore volume of PoPs are calculated to be decreased from bare MSN by 75.2% and 68.6%, respectively.

To investigate a drug retention effect of PoPs, a fluorescent dye of rhodamine 6G (Rh6G) was loaded onto the MSN by simply mixing the silica particles in an aqueous solution of Rh6G (5 mg/mL) overnight at 37 °C with vigorous shaking. Following repeated washing steps to remove unloaded dye with centrifugation, the dye-loaded MSN was coated with αSyn-AuNP of 5 nm in diameter as described above. The resulting Rh6G-loaded PoPs were dispersed in 10 mM Mes at pH 6.5 and then transferred to a dialysis device (Slide-A-lyzer MINI Dialysis, Thermo SCIENTIFIC) to remove incompletely entrapped or nonspecifically bound dyes and compare the drug retention efficiency of PoPs to that of bare MSN. According to the dye release profile from the Rh6G-loaded PoPs (Figure S4,e Supporting Information), the release of the dye was not observed after 2 h of dialysis. The amount of Rh6G entrapped inside increased linearly as the ratio of αSyn-AuNP/MSN (pmol/μg) increased, thereby indicating that the more αSyn-AuNPs were attached, the more dye was entrapped (Figure 4a). The dye retention by PoPs was confirmed to be not due to a possible molecular interaction between α-synuclein and Rh6G since they were shown to be readily separated without any tight complex formation as assessed with size-exclusion chromatography (Figure S5, Supporting Information). In fact, the extent of cargo retention increased as the plugging AuNP size decreased. The PoPs plugged with 5 nm αSyn-AuNP entrapped the dye six times as much as those with 10 nm αSyn-AuNP, and a negligible amount of dye was retained in the PoPs ornamented with 20 nm αSyn-AuNP (Figure 4b). By considering the AuNP packing density per MSN (see above), the exponentially augmented dye retention by 5 nm AuNP-PoPs might not be solely attributed to the small AuNP size. Hence, the protein of α-synuclein attached on AuNP could have played an additional role on holding the dye within MSN by acting alone or protein−protein interactions between the adjacent AuNPs. Therefore, the drug-loading capacity of PoPs can be improved by tuning the MSN pore diameter and/or the plugging nanoparticle size in the presence of α-synuclein.

As a physiologically relevant ligand for α-synuclein to control the gating behavior of PoP, Ca^{2+} was chosen to monitor the dye release since the cation was demonstrated to affect the amyloidogenesis of α-synuclein through specific molecular interaction.[25,26] Unlike other cations, most of which have been chelated under physiological conditions with biomolecules, the level of free Ca^{2+} remains relatively high and fluctuates in cytoplasm *via* tight regulation on the Ca^{2+} storing intracellular organelle of endoplasmic reticulum. More importantly, Ca^{2+} is not only a ubiquitous signaling ion involved in diverse cellular processes but also its spatial and temporal surges are implicated in the pathogenesis of various devastating diseases including cancer, neurodegenerative diseases, and cardiovascular disease.[27,28] Therefore, Ca^{2+} and its related signaling processes have been actively exploited as targets for drug development, and in the same context, we investigated the

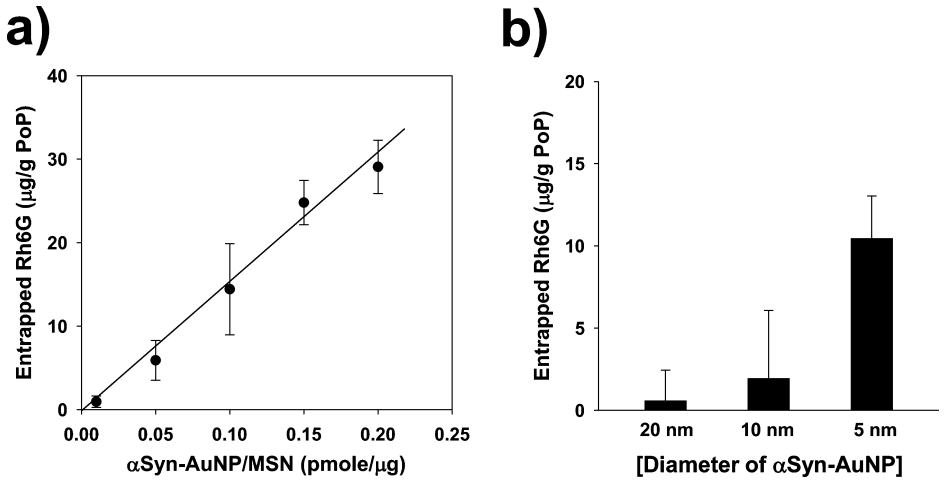

Figure 4. (a) Dye retention capacity of PoPs. PoPs were prepared with 50 μg of Rh6G-loaded MSN and various amounts of αSyn-AuNP (0.5, 2.5, 5, 7.5, and 10 pmol). At each ratio of αSyn-AuNP/MSN (pmol/μg), the amounts of entrapped Rh6G per g PoP were calculated and plotted after removing free and nonspecifically bound dye with dialysis. (b) αSyn-AuNP size-dependent retention of Rh6G within PoPs. Each Rh6G-loaded PoP was dialyzed for 2 h at room temperature, and then the fluorescence of dialyate was measured.

Ca^{2+}-responsive cargo release from the PoPs. As shown in Figure 5a, while the Rh6G-loaded PoPs did not leak in the absence of Ca^{2+}, the addition of 2 mM Ca^{2+} led to an abrupt initial increase of the dye fluorescence which in turn completed within 30 min, thereby indicating instantaneous release of the dye in response to the Ca^{2+} stimulation. This Ca^{2+}-triggered release was highly dependent upon the amount Ca^{2+} treated (Figure 5a inset). Since the ligand-induced conformation change of α-synuclein on αSyn-AuNP is suspected to be responsible for the dye-release from PoPs, we have employed the DLS analysis to monitor any change in the size of αSyn-AuNP in the presence of Ca^{2+}. In the absence of Ca^{2+}, the hydrodynamic diameter of αSyn-AuNP was 22.57 ± 0.46 nm. However, the diameter shrank to 20.51 ± 0.64 nm with 2 mM Ca^{2+} (Figure 5b). This ~2 nm change suggests that the α-synuclein on the surface of AuNP experiences conformational change with Ca^{2+}. It was also found that the αSyn-AuNPs remained tethered on the MSN surface after the dye release as assessed with a lack of the absorbance for αSyn-AuNPs in the supernatant collected after a centrifugation of the Ca^{2+}-treated PoPs and the TEM images of PoPs obtained before and after the Ca^{2+} treatment (Figure S6, Supporting Information). Therefore, the shrinkage of αSyn-AuNPs on PoPs could open the nanopores of MSN while the nanoparticles remain attached on the surface. When the PoPs were treated successively with increasing amounts of Ca^{2+} to the final concentrations of 0.5, 1, 2, and 4 mM, the Rh6G release responded in a stepwise manner, suggesting that the cargo release could be controlled intermittently (Figure 5c). This Ca^{2+}-triggered dye release was apparently not observed in the presence of calcium chelating agent, EDTA (Figure 5c). Taken together, these results indicated that the Ca^{2+}-induced conformational change of α-synuclein was responsible for unleashing the dye from PoPs not because of the actual detachment of αSyn-AuNPs from MSN but because of altered protein-MSN or protein–protein interactions on the MSN surface.

Other polyvalent (Cu^{2+}, Mg^{2+}, and Fe^{3+}) and monovalent cations (Na^{+} and K^{+}) were also tested to monitor their ability to release the dye from PoPs. In particular, those di- and trivalent cations have been suggested to bind the C- and/or partly N-terminal regions of α-synuclein, which would cause the conformational change and thus alter the fibrillation property of the protein.[29−31] The Rh6G-loaded PoPs were incubated in 20 mM Mes, pH 6.5, containing 2 mM of each cation for 10 min. The cation-triggered release of the dye was determined by monitoring the fluorescence of the supernatant following centrifugation (Figure 5d). A significant dye release was observed in the presence of Ca^{2+}, Cu^{2+}, Mg^{2+}, and Fe^{3+}. Cu^{2+} appeared to be the most effective ion, probably due to its high affinity to α-synuclein.[32] Therefore, our PoPs could be also developed into biosensors monitoring physiological/pathological levels of biologically important ions. Intriguingly, however, neither Na^{+} nor K^{+} was able to induce the dye release. It is this unresponsiveness of PoPs against the monovalent cations, the most abundant ions under the physiological condition, that is very significant in terms of avoiding untimely release of the loaded cargo from PoPs in biological fluids, and thus it may guarantee the drug-loaded PoPs to arrive at target sites safely without premature leakage. When the physiologically relevant polyvalent cations such as Ca^{2+} and metal ions bind to a protein, they are usually coordinated by electron rich atoms like nitrogen, oxygen, or sulfur comprising amino acid residues and peptide bonds, which is suggested to be the molecular basis of metal selectivity exerted by metal-binding proteins in general.[33] Ca^{2+} has been known to bind to the acidic C-terminal domain of α-synuclein, and

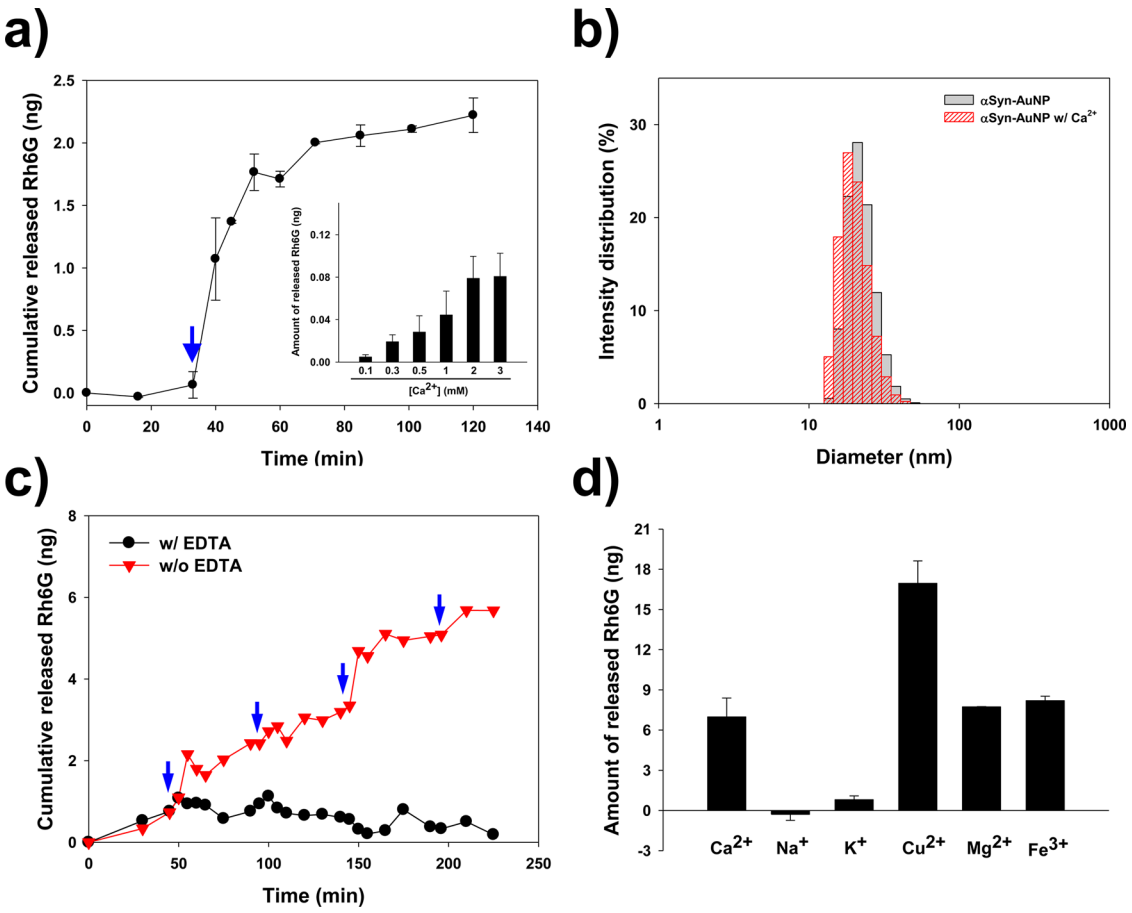

Figure 5. (a) Ca^{2+}-triggered Rh6G release from PoPs. Final 2 mM Ca^{2+} was added into the dialysate while monitoring a time-course release of the entrapped Rh6G within PoPs. The arrow indicates the point of Ca^{2+} addition. Inset: Ca^{2+} concentration-dependent Rh6G release from PoPs. (b) Hydrodynamic diameter of αSyn-AuNP in the presence or absence of Ca^{2+}. αSyn-AuNP was incubated in the presence of 2 mM Ca^{2+} for 30 min at room temperature, and then the change in the particle size distribution was measured by DLS. (c) Stepwise response of the dye release from PoPs. Final concentration of Ca^{2+} in the dialysate was increased every 50 min to 0.5, 1, 2, and 4 mM. The arrows indicate the points of Ca^{2+} addition. The experiment was performed in the absence or presence of 5 mM EDTA. (d) Effects of various cations on triggering the dye release from PoPs. Instead of Ca^{2+}, the Rh6G-loaded PoPs were incubated with 2 mM each of the mono- and polyvalent cations denoted for 10 min at room temperature.

an NMR study has revealed that copper ions bind to α-synuclein *via* the coordination of charged residues and backbone nitrogens.[25,34] Although molecular details are not clear, the coordination of polyvalent cations within and between α-synucleins on PoPs, possibly causing the conformational change of α-synuclein and thus the shrinkage of αSyn-AuNPs, could be responsible for the cargo release from PoPs as demonstrated with Ca^{2+} in Figure 5b. On the other hand, monovalent cations of Na^+ and K^+ could not be adequately coordinated within/between the proteins to induce a sufficient conformational change of the protein for the opening of nanopores on PoPs although they would interact with the acidic C-terminus of α-synuclein through charge interaction.

We have then investigated the Ca^{2+}-dependent intracellular drug release from PoPs loaded with anticancer drug of doxorubicin (DOX) in HeLa cells. The cellular uptake of PoPs was verified with confocal laser scanning microscope following the PoP treatment of HeLa cells for 1 h in PBS. Immuno-fluorescent staining with anti-αSyn antibody (LB509) revealed many fluorescent dots inside the HeLa cells, indicating rapid and successful internalization of the PoP nanostructures (Figure 6a). To examine the actual drug delivery of PoPs, the PoP_{DOX} loaded with the chemotherapeutic agent of doxorubicin was prepared. The UV−vis absorbance measurement indicated that 1 g of PoP contained approximately 6.12 mg of DOX. The cytotoxic effect of PoP_{DOX} was evaluated with HeLa cells after 18 h of incubation with various amounts of PoP_{DOX}. The result indicated that the cells died with PoP_{DOX} in a dose-dependent manner (Figure 6b). As a control, the empty PoPs at 100 μg without DOX loaded were confirmed to be not affecting the cell viability under the same condition (Figure S7, Supporting Information). In order to find out the Ca^{2+}-dependent cytotoxicity of PoP_{DOX} inside the cells, we used two well-established intracellular Ca^{2+}-regulating agents, BAPTA-AM (1,2-bis(o-aminophenoxy)ethane-*N*,*N*,*N*′,*N*′-tetraacetic acid, acetoxymethyl ester) and thapsigargin (TG). BAPTA-AM is the membrane-permeable

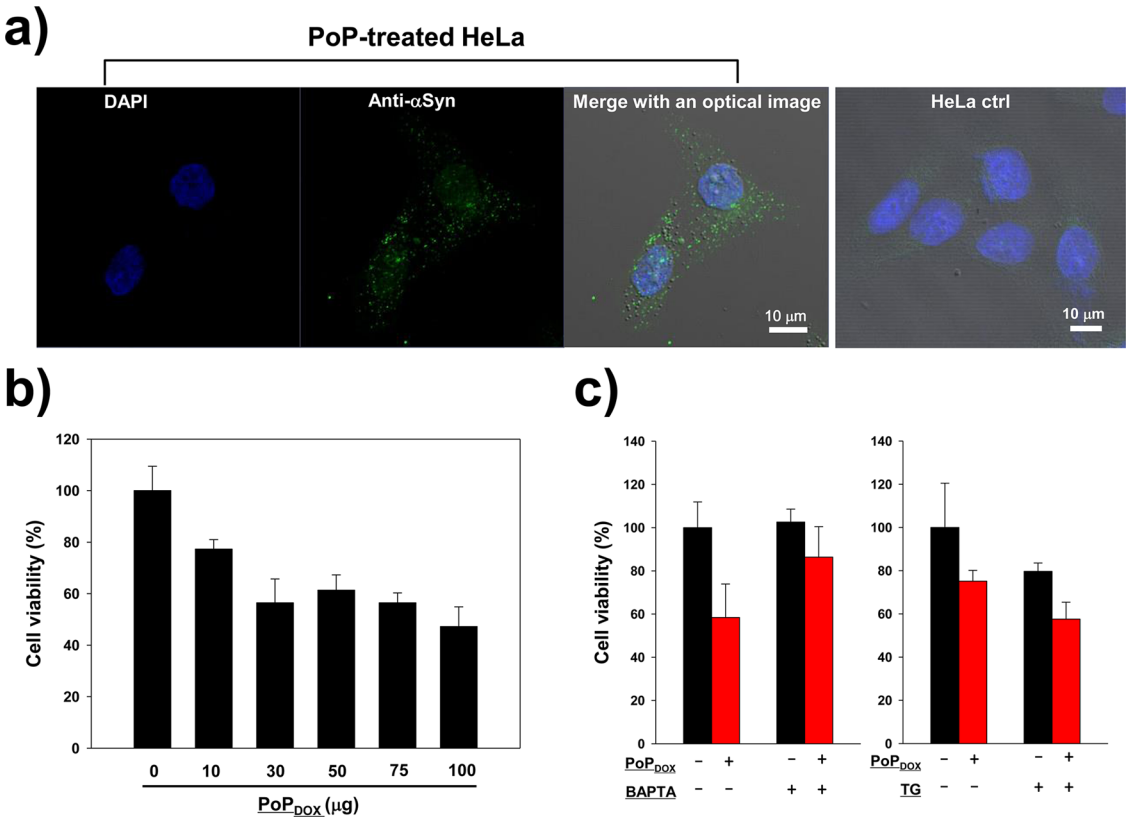

Figure 6. (a) Confocal images of HeLa cells containing PoPs. PoPs suspended in PBS was treated to HeLa cells for 1 h. Cells were stained with DAPI (blue) and anti-αSyn antibody (green). Both fluorescence images were merged with bright-field image. Merged image of nontreated HeLa cells (right end) was compared. (b) *In vitro* cytotoxicity of PoP_{DOX}. Various amounts of PoP_{DOX} were treated to HeLa cells grown to about 70% confluence. Total live cells were counted following incubating for 18 h. (c) Ca^{2+}-dependent cytotoxic effect of PoP_{DOX}. HeLa cells were incubated with 100 μg of PoP_{DOX} in the presence or absence of 50 μM BAPTA (left panel) and 50 μg of PoP_{DOX} in the presence or absence of 1 μM TG (right panel). Total live cells were counted following incubation for 18 h.

Ca^{2+} chelator that decreases cytosolic free Ca^{2+} concentration, whereas TG is the widely used inhibitor for the endoplasmic reticulum Ca^{2+} pump leading to an increase of cytosolic Ca^{2+} level.[35,36] The cytotoxicity exerted by PoP_{DOX} killing approximately 40% of the cells was reduced to 15% in the presence of BAPTA-AM at 50 μM, which was the concentration of BAPTA-AM hardly affecting the cell viability by itself. Furthermore, the PoP_{DOX} killed more cells in the presence of 1 μM TG by approximately 10% although the cytotoxicity of TG alone was comparable to that of PoP_{DOX} in the absence of TG (Figure 6c). Consequently, these results suggest that the internalized PoPs can respond to the change of intracellular Ca^{2+} level by controlling the release of its cargo molecules.

CONCLUSION

In this study, we have developed a novel MSN-based cargo delivery nanocomposite, named "raspberry-type" PoP, to which a protein ligand-responsive gate control system was introduced by employing the amyloidogenic and thus self-interactive α-synuclein and its physiological/pathological ligand of Ca^{2+}. *In vitro* cell studies demonstrated that the PoP nanocomposites were able to exert the efficient delivery and release of their entrapped chemotherapeutic agent of DOX, and therefore, its cytotoxic effect could be controlled by cytosolic Ca^{2+} level. Ongoing studies include optimization of the cargo entrapping efficiency and development of more precise spatiotemporal gate control system. Finally, we expect that these PoPs could be developed into a multifunctional smart delivery system for diverse theranostic purposes by incorporating various nanoparticles such as magnetic nanoparticles and Q-dots and derivatizing diverse bioactive molecules onto the exposed surface protein of α-synuclein.

METHODS

Materials. Cetyltrimethylamonium bromide (CTAB) and tetraethyl orthosilicate (TEOS) were purchased from Acros. Various diameters of gold nanoparticle (AuNP) were purchased from Sigma-Aldrich or BBI international. BAPTA-AM, TG, 4′,6-diamidino-2-phenylindole (DAPI), Rh6G, $CaCl_2$, $FeCl_3$, $MgCl_2$, and $CuCl_2$ were obtained from Sigma-Aldrich. Anti-αSyn (LB509) was purchased from Santa Cruz Biotechnology, and Alexafluoro 488-conjugated secondary antibody was purchased from Invitrogen.

Synthesis of Mesoporous Silica Nanoparticle (MSN). MSN was synthesized as described in the previous report.[24] Briefly, 50 mL of 0.2% CTAB solution was mixed with 0.35 mL of 2 M NaOH. The mixture was heated to 70 °C, followed by addition of 0.5 mL of TEOS. One minute later, 0.5 mL of ethyl acetate was added, and then the mixture was stirred for 30 s and incubated for 2 h at 70 °C. The precipitate was collected by centrifugation and washed with water and ethanol 4 times. Finally, CTAB was removed by refluxing in acidic ethanol solution. The morphology and size of the final nanoparticle were analyzed by TEM and DLS. For the preparation for particles-on-a-particle assembly and dye release assay, the ethanol-solubilizing MSN was exchanged with appropriate buffers by repeated equilibration and centrifugation several times.

Synthesis of αSyn-Immobilized AuNPs (αSyn-AuNPs). Cysteine mutants of αSyn replacing amino acid residues of serine at position 9, alanine at 53, and tyrosine at 136 with cysteine as denoted S9C, A53C, and Y136C, respectively, were synthesized according to the previous procedures using site-directed mutagenesis and *Escherichia coli* BL21 (DE3)-based overexpression system.[37] To construct αSyn-AuNPs, the cysteine mutant αSyn (final 14 μM) was mixed with 200 μL of AuNP colloids, and the mixture was incubated overnight at 4 °C. The cysteine mutant αSyn was conjugated to AuNP by making a covalent bond between the sulfhydryl group of cysteine and Au (Au−S). A molar ratio of αSyn/AuNP above 100 was determined to be sufficient to saturate the surface of nanoparticles with the protein. Actual molar ratio of αSyn/AuNP employed in the experiments turned out to be much higher than 100 like 15695, 1592, and 262 for 20, 10, and 5 nm of AuNP, respectively. The resulting reaction mixture was centrifuged for 1 h at 16100*g* to eliminate unbound proteins using a table-top centrifuge. The collected precipitate was washed with 200 μL of 20 mM Mes (pH 6.5) twice at the same centrifugal condition. The concentration of the final αSyn-AuNP was determined by the method described in the previous report.[38] Mostly, we obtained the purified αSyn-AuNPs whose concentration ranged from 0.3 to 0.5 nmol/mL for 5 nm AuNP, 0.08 to 0.11 nmol/mL for 10 nm AuNP, and 0.01 to 0.02 nmol/mL for 20 nm AuNP. The successful conjugation of α-synuclein to the surface of AuNP was verified by a flocculation test and observation of the corona of protein layer around the particles using TEM with 2% uranyl acetate staining. The flocculation test was performed by adding 150 mM NaCl to the solution containing αSyn-AuNPs, and the agglomeration of AuNPs was monitored using UV−vis spectrometer by scanning wavelength between 300 and 800 nm.

Particles-on-a-Particle (PoP) Assembly and Characterization. To assess an optimum condition for the maximum attachment of αSyn-AuNPs to MSN, the amount of αSyn-AuNPs was increased with a fixed amount of MSN (20 μg) during the incubation in 100 μL of 10 mM citrate at pH 4.4, and then the bound αSyn-AuNP per μg MSN was estimated (Figure S8, Supporting Information). As a matter of fact, αSyn-AuNP/MSN of 0.18 (pmol/μg) turned out to be sufficient for 5 nm particles to saturate MSN. As the AuNP size increased to 10 and 20 nm, the αSyn-AuNP/MSN ratio for the maximum particle attachment dropped to 0.037 and 0.017, respectively, which were estimated based on the same procedure performed for the 5 nm particles. Therefore, for all the preparation of PoPs done in this study, the ratio of αSyn-AuNP/MSN (pmol/μg) was maintained above the optimum values for the particles with different sizes to ensure the maximum incorporation of αSyn-AuNPs to MSN. In detail, MSN (50 μg or 100 μg) was mixed with 20 pmol of 5 nm αSyn-AuNP in a total reaction volume of 100 μL of 10 mM citrate buffer (pH 4.4). In the case of 10 and 20 nm αSyn-AuNP, 4 pmol and 2 pmol were added, respectively. The mixture was incubated for 30 min at room temperature. A red particulate was collected by centrifugation at 2300*g* for 10 min, and the resulting precipitates were dispersed by repeated pipetting in the buffer. The TEM images without staining were taken for confirming and analyzing nanostructures produced by particles-on-a-particle assembly. To confirm the hydrodynamic size distribution and stability of PoPs, the DLS analysis was carried out using the Zetasizer Nano (Malvern Instruments, Malvern, UK). The BET analysis using the ASAP 2020 Surface Area and Porosity Analyzer (Micrometrics, Cumming, GA) was employed to characterize the surface area and pore volume of the PoPs.

Dye Retention and Release Assay. A MSN solution (100 μL containing 4.35 mg of MSN) was added to 1 mL of 10 mM citrate buffer (pH 4.4) containing 1.5 mg/mL Rh6G, and the mixture was incubated overnight at 37 °C with vigorous shaking. After being washed several times with the buffer by using centrifugation at 2300*g* for 10 min, the combined Rh6G-loaded MSN was mixed with the appropriate amount of αSyn-AuNP in excess to obtain the dye-entrapped PoPs. The Rh6G-loaded PoPs were collected again and washed by using centrifugation at 2300*g* for 10 min. For DOX loading, the MSN solution (20 μL containing 1 mg of MSN) was added to 250 μL of 10 mM citrate buffer (pH 4.4) containing 2 mg/mL DOX. For the dye retention and release assay, 100 μg of Rh6G-loaded PoPs suspended in 100 μL of 20 mM Mes (pH 6.5) was transferred to a dialysis device (20K MWCO, 2 mL maximum volume, Slide-A-lyzer MINI Dialysis, Thermo SCIENTIFIC) floating in 6 mL of 20 mM Mes (pH 6.5) dialysis buffer. The constitutive and ion-responsive release of the dye were monitored by measuring fluorescence of the dialysis buffer at 552 nm (excited at 520 nm) at room temperature. To evaluate ion-responsive dye release from the PoPs, each ion was simply added to the dialysis buffer at the concentration indicated.

Cellular Internalization of PoPs and *in Vitro* Cytotoxicity. The HeLa cells were grown in Dulbecco's modified Eagle's medium supplemented with 10% (v/v) fetal bovine serum under 5% CO_2 at 37 °C. For the immunofluorescence analysis to demonstrate the cellular internalization of PoP nanocomposites, 1.8×10^4 cells were seeded in each coverslip-placed well of a 6-well plate and incubated for 24 h. PoP (25 μg) suspended in the phosphate-buffered saline (PBS) composed of 11.8 mM sodium/potassium phosphate, pH 7.4, and 0.14 M NaCl was added to each well in the medium growing cells, and the cells were incubated for another 3 h in 5% CO_2 at 37 °C. After washing with PBS to remove free PoPs, the cells growing on a coverslip were stained with anti-αSyn antibody, Alexafluoro 488-conjugated secondary antibody, and DAPI according to the manufacturer's instruction for immunofluorescence staining procedure. The fluorescence images were acquired using confocal laser scanning microscope. For *in vitro* cytotoxicity assay, 1.8×10^4 HeLa cells were seeded in a 24-well plate and grown until 70% confluence was reached. The indicated amounts of PoP and PoP_{DOX} were added to the media growing cells, and the cells were incubated for 18 h in 5% CO_2 at 37 °C. To examine the Ca^{2+}-dependent cytotoxicity of PoP_{DOX}, the cytotoxic effect of PoP_{DOX} was tested in the presence and absence of the indicated amounts of BAPTA or TG. After being washed with PBS and trypsinization, the total live cells were counted using a hematocytometer following trypan blue staining.

Conflict of Interest: The authors declare no competing financial interest.

Acknowledgment. This work was supported partly by the National Research Foundation of Korean (NRF) grants funded by the Ministry of Education (DL: 0458-20130016) and the Ministry of Science, ICT, and Future Planning (SRP: 2013029364).

Supporting Information Available: PoP assembly with the AuNPs immobilized with various mutant types of α-synuclein; detachment of αSyn-AuNPs from PoP nanocomposite; hydrodynamic size distribution of PoPs based on DLS analysis; dye-trapping capacity of PoPs; molecular interaction between α-synuclein and Rh6G; TEM images of PoPs obtained before and after the Ca^{2+} treatment; *in vitro* cytotoxicity of PoP and PoP_{DOX}; amount of αSyn-AuNPs bound to MSN. This material is available free of charge *via* the Internet at http://pubs.acs.org.

REFERENCES AND NOTES

1. Cheng, Z.; Al Zaki, A.; Hui, J. Z.; Muzykantov, V. R.; Tsourkas, A. Multifunctional Nanoparticles: Cost *Versus* Benefit of Adding Targeting and Imaging Capabilities. *Science* **2012**, *338*, 903–910.

2. Nie, S.; Xing, Y.; Kim, G. J.; Simons, J. W. Nanotechnology Applications in Cancer. *Annu. Rev. Biomed. Eng.* **2007**, *9*, 257–288.
3. Colilla, M.; González, B.; Vallet-Regí, M. Mesoporous Silica Nanoparticles for the Design of Smart Delivery Nanodevices. *Biomater. Sci.* **2013**, *1*, 114–134.
4. Tarn, D.; Ashley, C. E.; Xue, M.; Carnes, E. C.; Zink, J. I.; Brinker, C. J. Mesoporous Silica Nanoparticle Nanocarriers: Biofunctionality and Biocompatibility. *Acc. Chem. Res.* **2013**, *46*, 792–801.
5. Lu, J.; Liong, M.; Li, Z.; Zink, J. I.; Tamanoi, F. Biocompatibility, Biodistribution, and Drug-Delivery Efficiency of Mesoporous Silica Nanoparticles for Cancer Therapy in Animals. *Small* **2010**, *6*, 1794–1805.
6. He, Q.; Shi, J. Mesoporous Silica Nanoparticle Based Nano Drug Delivery Systems: Synthesis, Controlled Drug Release and Delivery, Pharmacokinetics and Biocompatibility. *J. Mater. Chem.* **2011**, *21*, 5845–5855.
7. Chen, Y.; Chen, H.; Shi, J. *In Vivo* Bio-Safety Evaluations and Diagnostic/Therapeutic Applications of Chemically Designed Mesoporous Silica Nanoparticles. *Adv. Mater.* **2013**, *25*, 3144–3176.
8. Lee, J. E.; Lee, N.; Kim, T.; Kim, J.; Hyeon, T. Multifunctional Mesoporous Silica Nanocomposite Nanoparticles for Theranostic Applications. *Acc. Chem. Res.* **2011**, *44*, 893–902.
9. Lee, C.-H.; Cheng, S.-H.; Huang, I.-P.; Souris, J. S.; Yang, C.-S.; Mou, C.-Y.; Lo, L.-W. Intracellular pH-Responsive Mesoporous Silica Nanoparticles for the Controlled Release of Anticancer Chemotherapeutics. *Angew. Chem., Int. Ed.* **2010**, *49*, 8214–8219.
10. Slowing, I. I.; Vivero-Escoto, J. L.; Wu, C.-W.; Lin, V. S.-Y. Mesoporous Silica Nanoparticles as Controlled Release Drug Delivery and Gene Transfection Carriers. *Adv. Drug Delivery Rev.* **2008**, *60*, 1278–1288.
11. Park, C.; Oh, K.; Lee, S. C.; Kim, C. Controlled Release of Guest Molecules from Mesoporous Silica Particles Based on a pH-Responsive Polypseudorotaxane Motif. *Angew. Chem., Int. Ed.* **2007**, *46*, 1455–1457.
12. Hong, C.-Y.; Li, X.; Pan, C.-Y. Fabrication of Smart Nanocontainers with a Mesoporous Core and a pH-Responsive Shell for Controlled Uptake and Release. *J. Mater. Chem.* **2009**, *19*, 5155–5160.
13. Kim, H.; Kim, S.; Park, C.; Lee, H.; Park, H. J.; Kim, C. Glutathione-Induced Intracellular Release of Guests from Mesoporous Silica Nanocontainers with Cyclodextrin Gatekeepers. *Adv. Mater.* **2010**, *22*, 4280–4283.
14. Gruenhagen, J. A.; Lai, C.-Y.; Radu, D. R.; Lin, V. S.-Y.; Yeung, E. S. Real-Time Imaging of Tunable Adenosine 5-Triphosphate Release from an MCM-41-Type Mesoporous Silica Nanosphere-Based Delivery System. *Appl. Spectrosc.* **2005**, *59*, 424–431.
15. Mal, N. K.; Fujiwara, M.; Tanaka, Y. Photocontrolled Reversible Release of Guest Molecules from Coumarin-Modified Mesoporous Silica. *Nature* **2003**, *421*, 350–353.
16. Chen, P.-J.; Hu, S.-H.; Hsiao, C.-S.; Chen, Y.-Y.; Liu, D.-M.; Chen, S.-Y. Multifunctional Magnetically Removable Nanogated Lids of Fe_3O_4-Capped Mesoporous Silica Nanoparticles for Intracellular Controlled Release and MR Imaging. *J. Mater. Chem.* **2011**, *21*, 2535–2543.
17. Lai, C.-Y.; Trewyn, B. G.; Jeftinija, D. M.; Jeftinija, K.; Xu, S.; Jeftinija, S.; Lin, V. S.-Y. A Mesoporous Silica Nanosphere-Based Carrier System with Chemically Removable CdS Nanoparticle Caps for Stimuli-Responsive Controlled Release of Neurotransmitters and Drug Molecules. *J. Am. Chem. Soc.* **2003**, *125*, 4451–4459.
18. Gan, Q.; Lu, X.; Yuan, Y.; Qian, J.; Zhou, H.; Lu, X.; Shi, J.; Liu, C. A Magnetic, Reversible pH-Responsive Nanogated Ensemble Based on Fe3O4 Nanoparticles-Capped Mesoporous Silica. *Biomaterials* **2011**, *32*, 1932–1942.
19. Liu, R.; Zhang, Y.; Zhao, X.; Agarwal, A.; Mueller, L. J.; Feng, P. pH-Responsive Nanogated Ensemble Based on Gold-Capped Mesoporous Silica through an Acid-Labile Acetal Linker. *J. Am. Chem. Soc.* **2010**, *132*, 1500–1501.
20. Sun, X.; Zhao, Y.; Lin, Victor S.-Y.; Slowing, I. I.; Trewyn, B. G. Luciferase and Luciferin Co-immobilized Mesoporous Silica Nanoparticle Materials for Intracellular Biocatalysis. *J. Am. Chem. Soc.* **2011**, *133*, 18554–18557.
21. Martin-Ortigosa, S.; Valenstein, J. S.; Lin, V. S.-Y.; Trewyn, B. G.; Wang, K. Gold Functionalized Mesoporous Silica Nanoparticle Mediated Protein and DNA Codelivery to Plant Cells *via* the Biolistic Method. *Adv. Funct. Mater.* **2012**, *22*, 3576–3582.
22. Volles, M. J.; Lansbury, P. T., Jr. Zeroing in on the Pathogenic Form of α-Synuclein and Its Mechanism of Neurotoxicity in Parkinson's Disease. *Biochemistry* **2003**, *42*, 7871–7878.
23. Lee, D.; Choe, Y.-J.; Lee, M.; Jeong, D. H.; Paik, S. R. Protein-Based SERS Technology Monitoring the Chemical Reactivity on an α-Synuclein-Mediated Two-Dimensional Array of Gold Nanoparticles. *Langmuir* **2011**, *27*, 12782–12787.
24. Lee, J. E.; Lee, N.; Kim, H.; Kim, J.; Choi, S. H.; Kim, J. H.; Kim, T.; Song, I. C.; Park, S. P.; Moon, W. K.; Hyeon, T. Uniform Mesoporous Dye-Doped Silica Nanoparticles Decorated with Multiple Magnetite Nanocrystals for Simultaneous Enhanced Magnetic Resonance Imaging, Fluorescence Imaging, and Drug Delivery. *J. Am. Chem. Soc.* **2010**, *132*, 552–557.
25. Lowe, R.; Pountney, D. L.; Jensen, P. H.; Gai, W. P.; Voelcker, N. H. Calcium(II) Selectively Induces α-Synuclein Annular Oligomers *via* Interaction with the C-terminal Domain. *Protein Sci.* **2004**, *13*, 3245–3252.
26. Nath, S.; Goodwin, J.; Engelborghs, Y.; Pountney, D. L. Raised Calcium Promotes α-Synuclein Aggregate Formation. *Mol. Cell. Neurosci.* **2011**, *46*, 516–526.
27. Monteith, G. R.; McAndrew, D.; Faddy, H. M.; Roberts-Thomson, S. J. Calcium and Cancer: Targeting Ca^{2+} Transport. *Nat. Rev. Cancer.* **2007**, *7*, 519–530.
28. Leal, S. S.; Botelho, H. M.; Gomes, C. M. Metal Ions as Modulators of Protein Conformation and Misfolding in Neurodegeneration. *Coord. Chem. Rev.* **2012**, *256*, 2253–2270.
29. Uversky, V. N.; Li, J.; Fink, A. L. Metal-Triggered Structural Transformations, Aggregation, and Fibrillation of Human α-Synuclein: a Possible Molecualr Link Between Parkinson's Disease and Heavy Metal Exposure. *J. Biol. Chem.* **2001**, *276*, 44284–44296.
30. Tamamizu-Kato, S.; Kosaraju, M. G.; Kato, H.; Raussens, V.; Ruysschaert, J.-M.; Narayanaswami, V. Calcium-Triggered Membrane Interaction of the α-Synuclein Acidic Tail. *Biochemistry* **2006**, *45*, 10947–10956.
31. Sung, Y.-H.; Rospigliosi, C.; Eliezer, D. NMR Mapping of Copper Binding Sites in Alpha-synuclein. *BBA-Proteins Proteomics* **2006**, *1764*, 5–12.
32. Bisaglia, M.; Tessari, I.; Mammi, S.; Bubacco, L. Interaction Between α-Synuclein and Metal Ions, Still Looking for a Role in the Pathogenesis of Parkinson's Disease. *Neuromol. Med.* **2009**, *11*, 239–251.
33. Harding, M. M. The Architecture of Metal Coordination Groups in Proteins. *Acta. Crystallogr. D Biol. Crystallogr.* **2004**, *60*, 849–859.
34. Binolfi, A.; Quintanar, L.; Bertoncini, C. W.; Griesinger, C.; Fernández, C. O. Bioinorganic Chemistry of Copper Coordination to Alpha-synuclein: Relevance to Parkinson's Disease. *Coord. Chem. Rev.* **2012**, *256*, 2188–2201.
35. Zhou, S.; Yuan, X.; Liu, Q.; Zhang, X.; Pan, X.; Zang, L.; Xu, L. BAPTA-AM, an Intracellular Calcium Chelator, Inhibits RANKL-Induced Bone Marrow Macrophage Differentiation through MEK/ERK, p38 MAPK and Akt, but not JNK Pathways. *Cytokine* **2010**, *52*, 210–214.
36. Jan, C.-R.; Ho, C.-M.; Wu, S.-N.; Tseng, C.-J. Mechanism of Rise and Decay of Thapsigargin-Evoked Calcium Signals in MDCK Cells. *Life Sci.* **1999**, *64*, 259–267.
37. Lee, D.; Choe, Y.-J.; Choi, Y. S.; Bhak, G.; Lee, J.; Paik, S. R. Photoconductivity of Pea-Pod-Type Chains of Gold Nanoparticles Encapsulated within Dielectric Amyloid Protein Nanofibrils of α-Synuclein. *Angew. Chem., Int. Ed.* **2011**, *50*, 1332–1337.
38. Haiss, W.; Thanh, N. T. K.; Aveyard, J.; Fernig, D. G. Determination of Size and Concentration of Gold Nanoparticles from UV−Vis Spectra. *Anal. Chem.* **2007**, *79*, 4215–4221.